Water Air Soil Pollut (2025) 236:742
https://doi.org/10.1007/s11270-025-08323-1

Effect of Cellulose Nanofibril Size on Adsorption Behavior of 3-D Cellulose Hydrogels

Yufei Nan · Diego Gomez-Maldonado · Fatimatu Bello · J. Y. Zhu · Maria Soledad Peresin

Received: 10 April 2025 / Accepted: 1 July 2025

Abstract With the development of cellulose nanofibril (CNF)-based adsorbents, the influence of particle size on adsorption capability has become increasingly recognized. In this study, endoglucanase FiberCare® was utilized to decrease fibril size of TEMPO-oxidized cellulose nanofibrils (TCNFs) without changing carboxyl groups content of the resulting TCNFs. Average fibril length decreased by 27.3% (from 508.7 nm to 369.4 nm) after enzymatic hydrolysis for 12 h and further decreased by 35.4% (to 328.2 nm) after 24 h. Meanwhile, the average fibril diameter decreased 20.2% (from 56.8±16.3 to 45.3±14.3) after 12 h of hydrolysis, further reduced by 32.6% (to 38.3±13.1 nm) after 24 h. Carboxyl group content remained unchanged. Zeta potential of the TCNFs was increased by 5.5 mV after 24 h hydrolysis due to the exposure of more hydroxyl groups as fibril size decreases. TCNF hydrogel (from 12 h hydrolyzed) showed 20.3% increase in adsorption of cationic methylene blue dyes (from 64 mg/g to 77 mg/g) compared to untreated samples. However, further fibril size reduction after 24 h hydrolysis did not improve adsorption capability. Kinetic analysis using pseudo-second-order kinetic model and intra-particle diffusion model revealed no change in the adsorption mechanism, though the overall adsorption rate increased. This study highlights that reducing fibril size can enhance both adsorption capacity and rate, offering guidance for the design of CNF-based adsorbents.

Keywords Cellulose nanofibrils · Particle size · Adsorption capability · Adsorption rate · Electrostatic attraction

Supplementary Information The online version contains supplementary material available at https://doi.org/10.1007/s11270-025-08323-1.

Y. Nan · D. Gomez-Maldonado · F. Bello · M. S. Peresin (✉)
Sustainable Bio-Based Materials Laboratory, College of Forestry, Wildlife and Environment, Auburn University, 602 Duncan Drive, Auburn, AL 36849, USA
e-mail: speresi@clemson.edu

J. Zhu
USDA Forest Service, Forest Products Laboratory, Madison, WI, USA

M. S. Peresin
Wood Utilization and Design Institute, Clemson University, Clemson, United States

1 Introduction

Cellulose nanofibrils (CNFs) are obtained from abundant and renewable biomass resources. They have unique morphology and functionality characteristics when compared to petroleum-based nanomaterials (Isogai, 2021). With current concerns over the environment such as climate change and microplastics in marine and terrestrial environments, as well as emerging contaminants, the incorporation of

Published online: 29 July 2025

cellulose-based nanomaterials such as CNF to commodity and high-tech materials is expected to contribute to establishing sustainable society and circular economy (Habibi et al., 2010; Isogai, 2021).

CNFs are cellulose fibrils with diameters approximately 4 to 100 nm (Kaur et al., 2021; Khalid et al., 2021). CNFs can be isolated from plant cellulosic fibers via mechanical fibrillation with or without chemical or enzymatic pretreatments (Zhu and Agarwal, 2022). The strong interfibrillar hydrogen bonds among cellulose microfibrils are a challenge to achieve complete separation of CNF even with large energy input (Hoeger et al., 2013). However, the particle size of CNF plays a crucial role in determining the properties and performance in various applications (Hubbe et al., 2008; Zhu et al., 2016). Smaller fibril diameters are advantageous for making films with greater optical transparency (Nogi et al., 2009), and better barrier performance for packaging (Nair et al., 2014). When applied to reinforce polar matrices such as epoxy resin, starch, PLA, etc., smaller diameter fibrils also result in better mechanical properties (Hubbe and Grigsby, 2020; Sehaqui et al., 2013).

It is noteworthy that the fibril size (most of studies focus on fibril diameter) or surface area of CNF significantly influences its adsorption because surface area dictates adsorption capability and adsorption rate (Esmaeili et al., 2021). For example, CNF had a significantly greater adsorption capability of 14 mg/g for copper ions compared with microcrystalline cellulose of 0.02 mg/g, or a 700-fold increase (Qiao et al., 2021). Generally, a larger specific surface area means more adsorption sites which leads to a greater adsorption capability (Yang et al., 2011, Esmaeili et al. 2021). Cellulose nanoparticles hold specific surface area in the range of 50 to 200 m^2/g (Mishra et al., 2018). Moreover, fibril size also influences the resulting porous structure of CNF assemblies, which in term affects the adsorption efficiency, *e.g.* narrower micropores can enhance the adsorpition capability through the filling mechanism, leading to the accumulation of target pollutants in the channels (Zhang et al., 2016, Yu et al., 2020). When the pollutants diffuse into the channels, intraparticle diffusion dominates. In this case, narrow pores will impede the diffusion process and result in slower adsorption kinetics (Zhang et al., 2016, Zhang et al., 2023). Therefore, it is interesting to understand how CNF fibril size affects adsorption kinetics of CNF assembled 3-D structure.

Limited studies were carried out using CNF-based 3-D structural adsorbents when investigating the effect of CNF fibril size on absorption performance. This work was aimed at investigating the effect of fibril size (both fibril length and fibril diameter) of TEMPO (2,2,6,6-Tetramethylpiperidin-1-oxyl)-oxidized cellulose nanofibril (TCNF) on adsorption behavior of 3-D TCNF assembly. Enzymatic pretreatment of TCNF using a commercial endoglucanase (FiberCare®, Novozymes) was carried out to obtain TCNFs with varied lengths and diameter followed assembly into 3-D hydrogels by cationic coordination. The cationic dye absorption capacities of the hydrogels made from endoglucanase treated TCNFs were evaluated using methylene blue. This work contributes relevant basic knowledge to designing efficient adsorbents using cellulose nanomaterials.

2 Materials and Methods

2.1 Materials

CNF from bleached soybean hulls was produced by mechanical processing at the Sustainable Bio-based Materials Lab at Auburn University, Alabama, as described in a previous study (Bello and Peresin, 2024). Briefly, a 2 wt.% bleached soyhull cellulose fiber suspension was defibrillated in a Masuko supermasscolloider (MKZA10-15J, Masuko Sangyo Co., Fiber Japan) until a gel-like suspension was formed. This suspension was subsequently stored at 4 °C until use. Polyethylenimine (branched, Mw = 25,000 g/mol) was purchased from Sigma-Aldrich. TEMPO, and methylene blue cationic (MB) dye was purchased from VWR. A commercial endoglucanase, FiberCare®, was complimentarily provided by Novozymes, North America (Franklinton, NC, United States). The protein content of FiberCare® was assayed at 7.53 mg/mL according to a literature method (Bradford, 1976). The NaBr (97%) and NaClO (12.5%) were all purchased from VWR.

2.2 Preparation of TCNF

TEMPO-mediated oxidation of CNF was done as previously reported (Saito and Isogai, 2004; Nan

et al., 2023a). Briefly, 5 g of CNFs (dry mass basis) was dispersed into 500 mL distilled water that contained 0.08 g TEMPO (0.1 mmol/g CNF) and 0.5 g NaBr (1 mmol/g CNF). The pH of the solution was then adjusted to 10 using 0.5 M NaOH. This was followed by the slow addition of approximately 30 mL of 12.5% NaClO solution to the CNF slurry at 0.165 mL/min for a period of 3 h and the reaction was maintained at pH 10.5 at room temperature by simultaneously adding 0.5 M NaOH. The oxidized CNFs were precipitated after adding ethanol (1500 mL) and then centrifuged at 3,800 rpm for 3 h. Finally, the TEMPO-oxidized CNFs (TCNF) were washed thoroughly with distilled water until conductivity was the same as distilled water and filtered using a 0.20 µm cellulose acetate filter paper and stored at 4 °C.

2.3 Endoglucanase Treatment of TCNF

The endoglucanase treatment of TCNF to obtain different fibril lengths and diameters was carried out according to the procedure described by Wang et al. (2020). A TCNF dispersion at approximately 2 wt.% was treated with FiberCare® at 0.4 mg protein/g TEMPO-CNF in an acetate buffer solution of pH 4.8 for 12 and 24 h at 50 °C. The enzymes were deactivated by boiling the mixture for 5 minutes in a water bath at the end of preset hydrolysis times. Finally, samples were washed with DI water and centrifuged at 3,800 rpm for 3 h until conductivity was the same as DI water. Finally, the samples were stored in a refrigerator at 4 °C until use.

2.4 TCNF Hydrogel Formation and Functionalization with PEI

TCNF hydrogels were prepared by adding 0.35 mL of 20 wt.% $ZnCl_2$ solution dropwise along the walls of a glass container into a 1.5 wt.% aqueous TCNF dispersion. The mixture was allowed to stand for 24 h without stirring to enable the formation of the hydrogels. Afterward, unreacted Zn^{2+} ions were removed by rinsing the resulting hydrogels with 150 mL of distilled water three times. Then the washed TCNF hydrogels were immersed in 20 % of PEI solution with pH 11.7 for 24 h to functionalize and form the TCNF/PEI hydrogels.

2.5 Characterization

2.5.1 Atomic Force Microscopy (AFM)

The morphology of TCNFs was characterized using Tosca 400 equipment from Anton-Paar (Gratz, Austria). Each sample of CNF and TCNF was first spin-coated on a silicon wafer at 3,000 rpm for 30 s using 150 µL of 0.01% aqueous suspension in an area of 1.5×1.5 cm^2. Height images of the coated CNF or TCNF were obtained by atomic force microscopy (AFM) in tapping mode using a Nanoworld (Neuchâtel, Switzerland) ARROW-NCR-20 silicon SPM-sensor cantilever at a resonance frequency of 285 kHz and constant force of 42 N/m. The scan size was 5×5 μm^2. Processing of the images was accomplished by Gwyddion software 2.49 (SourceForge), and the heights of fibrils were calculated using ImageJ (KLA Corporation, Milpitas, CA, U.S.).

2.5.2 Carboxyl Content Determination

The carboxyl content of TCNF was determined by conductometric titrations based on a modified method from literature (Saito et al., 2009). Briefly, 30 mg (dry basis) of TCNF samples were suspended in 7.5 mL of 0.01 M HCl solution and the pH was adjusted to pH 2. After 2 h of stirring, the suspensions were titrated with 0.01 M NaOH, and the carboxyl content (mmol/g TCNF) was calculated using the following equation:

$$Carboxyl\ content = \frac{cV}{m} \times 1000 \quad (1)$$

c (mol/L) is NaOH concentration, V (L) is NaOH amount consumed to neutralize the weak acid, i.e., carboxylate groups, m (g) is weight of dry based TCNF.

2.5.3 Dynamic Light Scattering (DLS)

The zeta potential of 0.1 wt.% TCNF (after 12 and 24 h hydrolysis) and PEI solutions were tested in a pH range from 2 to 12. All measurements were conducted using a Litesizer DLS 500 (Anton-Paar, Gratz, Austria) at room temperature. For all samples, twelve

replicates were carried out and average data was reported.

2.5.4 Scanning Electron Microscopy (SEM)

Freeze-dried hydrogels were set onto aluminum stubs and sputter coated with gold for 90 s in an EMS ×550 Sputter coating device from Science Services (Munich, Germany). SEM images with magnifications of ×50, ×100, and ×1000 was then recorded in a Zeiss Evo 50VP SEM (Oberkochen, Germany).

2.5.5 Elemental Analysis

Elemental analysis was performed on each freeze-dried hydrogel using an elemental analyzer (Elementar vario MICRO, Ronkonkoma, NY, USA). Approximately 2 mg of freeze-dried sample was used for the test, and all measurements were performed in triplicate.

2.5.6 Adsorption of Methylene Blue Dyes

The adsorption of cationic methylene blue by different TCNF hydrogels was performed following the method described in the literature (Nan et al., 2024). A 0.0186 g of hydrogel was immersed into 10 mL of 200 mg/L methylene blue cationic dye solutions at different pH 3.7-9.7 for 24 h to determine the optimal pH value for maximum adsorption. Time-dependent adsorption was obtained by taking aliquots at different absorption times. The adsorption data were fitted to the pseudo-first-order kinetic model, pseudo-second-order kinetic model, and intra-particle diffusion model, using the equations presented below:

$$Ln\left(q_{e-}q_t\right) = Lnq_e + k_1\mathrm{t} \tag{2}$$

$$\frac{t}{q_t} = \frac{t}{k_2 q_e^2} + \frac{t}{q_e} \tag{3}$$

$$q_t = K_{id}t^{0.5} + \mathrm{c} \tag{4}$$

where k_1 and k_2 are the rate constants for the pseudo-first-order adsorption and pseudo-second-order adsorption kinetic models, respectively. K_{id} is the rate constant (g mg^{-1} min^{-1}) of intra-particle diffusion kinetics, c is intercept.

2.6 Statistical Analysis

One-way analysis of variance (ANOVA) followed by a post-hoc (Turkey HSD Test) was used to determine the significant difference among group means. Differences among mean values were considered significant when the probability value $p \leq 0.05$.

3 Results and Discussion

3.1 Effect of Enzymatic Hydrolysis on TCNF Particle Size

The changes in TCNF fibril size by endoglucanase treatment were revealed by AFM imaging and between 259-300 fibers were measured by ImageJ for average fiber length, diameter calculation, and statistical analysis. As shown in Fig. 1, the average fibril length and diameter were decreased by 27.3%, i.e., from 508.7 ± 20.8 nm to 369.4 ± 12.1 nm, and 20.2%, i.e., from 56.8±16.3 to 45.3±14.3 after 12 h of hydrolysis, respectively, and were further decreased by 35.4%, to 328.2 ± 12.6 nm and 32.6% to 38.3±13.1 nm after 24 h. This is a result of effective cleavage of the glycosidic bonds in the less ordered regions of the cellulose nanofibrils (Wang et al., 2020). Tukey HSD Test was applied to determine the statistical significance of the differences in fibril length and diameter among the TCNF samples. The results listed in Table 1 indicate that endoglucanase treatment effectively decreased TCNF fibril length and diameter. Similar trend was reported by Wang et al. (2020) when they studied the effect of FiberCare® treatment on fibril diameter represented by the AFM measured image height of lignin-containing CNF produced by maleic acid hydrotropic fractionated birch wood fibers (Wang et al., 2020). Compared with previous research (Wang et al., 2020), in our work, TCNF fibril size (both length and diameter) decreased more rapidly after hydrolysis by FiberCare®, which may be caused by TEMPO-mediated oxidation processing. As a result, the nanocellulose fibril size decreased more (Kapoor et al., 2019).

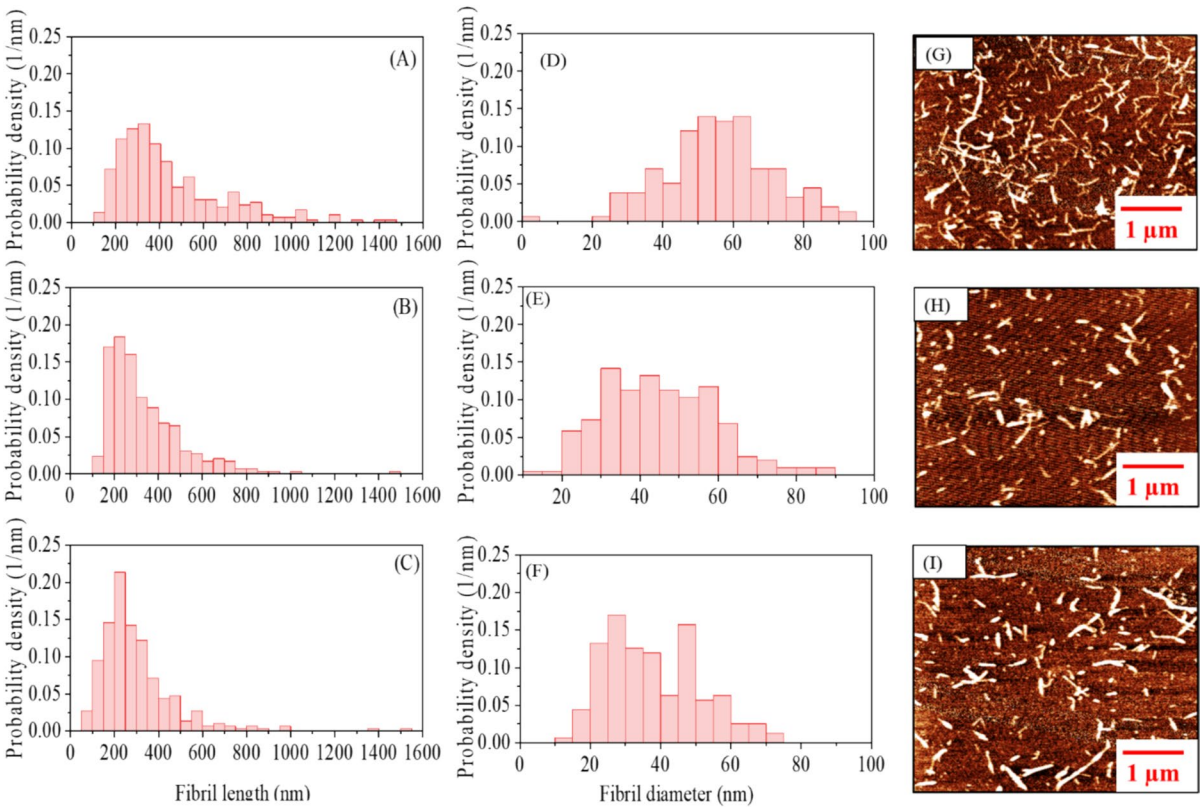

Fig. 1 Histograms of fibril size distribution and AFM images of cellulose nanocrystal hydrolyzed by endoglucanase. **A**, **D** and **G** show the control sample (0 h); **B**, **E** and **H** show the fibrils length change after 12 h hydrolysis; and **C**, **F** and **I** are fibril height obtained after 24 h enzymatic hydrolysis. Overall, a decrease in average fibril length and diameter was shown as hydrolysis time increased

Table 1 Average fiber length and fibril diameter after 0, 12, and 24 h of hydrolysis, and Tukey HSD test for log transformation data to compare the difference of average fiber length. The carboxyl group content for all the TCNF after hydrolysis was tested. Each test was done by triplicates; averages and standard deviations were reported

Treatment time	0 h	12 h	24h
Average fibril length (nm)	508.7 ± 20.8^{a} ($p_{ab}<0.05$)	369.4 ± 12.1^{b} ($p_{bc}<0.05$)	328.2 ± 12.6^{c} ($p_{ac}<0.05$)
Average fibril diameter (nm)	56.8 ± 16.3^{A} ($p_{AB}<0.05$)	45.3 ± 14.3^{B} ($p_{BC}<0.05$)	38.3 ± 13.1^{C} ($p_{AC}<0.05$)
Carboxyl group content (mmol/g TCNF)	1.5±0.01	1.5±0.02	1.5±0.05

3.2 Effect of TCNF Fibril Dimensions on Carboxyl Content and Zeta Potential

Endoglucanase treatment resulted in significant decreases in both the fibril length and diameter as shown in Fig. 1, however, the carboxyl group contents of TCNFs remained at 1.5 mmol/g TCNF (dry basis) (Table 1), confirming that the endoglucanase treatment did not introduce new carboxyl groups onto fibrils. The zeta potential is a key indicator of the surface charge and colloidal stability of TCNF and plays a crucial role in their functionalization and adsorption capabilities in hydrogel systems. The results show that the zeta potential of TCNF (absolute values) increased as the fibril length or diameter decreased. Specifically, the absolute value of zeta potential was

greatly increased from 42.6 mV to 48.1 mV at pH 5.7, and from 38.7 mV to 42.6 mV at pH 11.7, when the average fibril length decreased from 508.7±20.8 to 369.4±12.1 with diameter decreased from 56.8±16.3 to 45.3±14.3 (Fig. 2). These results agree with literature that reported LCNF zeta potential was increased from 33.5 mV to 44.5 mV when the fibril diameter decreased from 693 to 649 nm (Wang et al., 2020). This increase in zeta potential may be attributed to a higher number of surface hydroxyl groups, which result from the cleavage of longer cellulose chains into a greater number of shorter chains.

3.3 Effect of Fibril Size on Surface Properties and Adsorption Behavior of Hydrogels

3.3.1 Effect of Fibril Size on Surface Functionalization Capability

Based on our previous research (Nan et al., 2023a), PEI-functionalized CNF hydrogel exhibited a high adsorption capability for multiple water pollutants. Moreover, the adsorption capability was increased with the increase in the number of amine groups (Nan et al., 2023b). The amount of amine groups introduced onto the functionalized TCNF-based adsorbents are correlated with the TCNF zeta potential, carboxyl groups content, as well as fibril size. Among these variables, the effect of fibril size has often been overlooked. Because the cost of CNF production depends on fibrils size, it is of great importance to understand the effect of fibril size on the absorption capacity of hydrogels made of PEI functionalized for optimizing the design of more efficient cellulose-PEI adsorbents. The TCNF fibril size did not exhibit statistically significant effect ($p>0.05$) on PEI immobilization onto the TCNF hydrogel surface based on nitrogen analysis as shown in Fig. 2B. This is because PEI immobilization on TCNF is mainly controlled by hydrogen bonding and/or electrostatic attraction. The difference in fibril size among the tested TCNFs may not be substantial enough to affect these two mechanistic parameters.

3.3.2 The Effect of Fibril Size on TCNF Hydrogel Morphological Properties

Fibril size has been reported to be a crucial factor in controlling the morphology of hydrogels during its 3-D assembly through lyophilization (Gu et al., 2015). Smaller fibril size forms a smooth surface with homogeneous characteristic throughout the layer structure (Han et al., 2013). In this work, the focus is on the effect of fibril size on the morphology of hydrogel

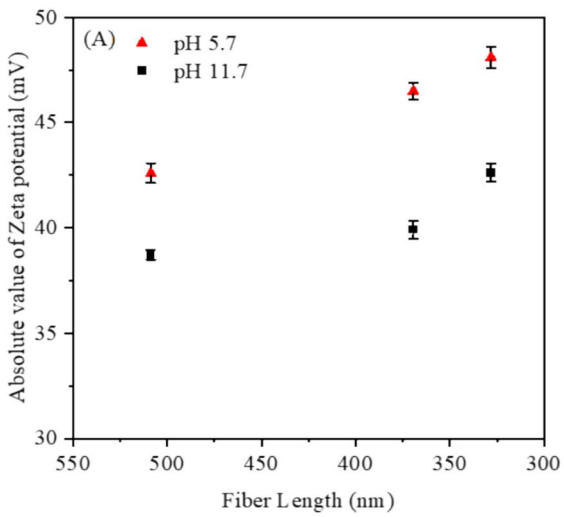

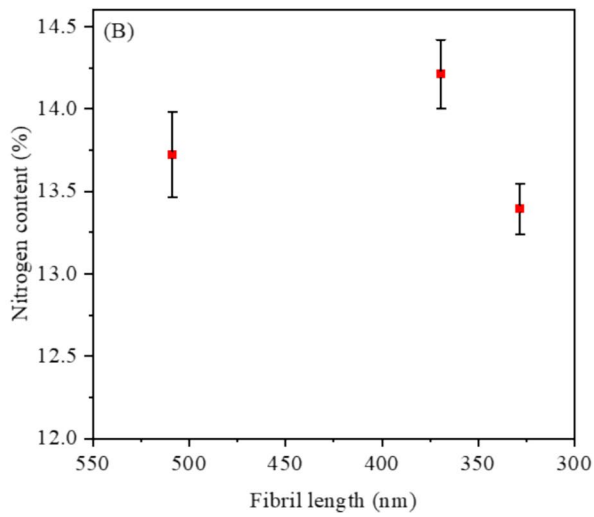

Fig. 2 **A** The zeta potential change of CNF with different fibril size after enzymatic hydrolysis for 12 and 24 h at pH 5.7 and 11.7 (the former is the pH of adsorption, and the latter is the pH of PEI functionalization. Standard deviations are < 0.5). **B** Effect of particle size on the PEI immobilization on TCNF hydrogel surface. Each test was done by triplicates; averages and standard deviations were reported

assemblies induced by cationic coordination and adsorption of PEI on the surfaces. The morphological properties of the hydrogels were observed by SEM as shown in Fig. S1. The hydrogels formed using endoglucanase treated TCNFs exhibited a more porous structure than the hydrogel formed with TCNF without endoglucanase treatment, in agreement with the work by Han et al., 2013. However, there is no significant difference when the fibril length decreased from 369.4 nm to 328.2 nm or fibril diameter decreased from 45.3 nm to 38.3 nm, maybe due to this fibril size changed range were not enough to make morphology properties change.

3.3.3 *Effect of pH and Fibril Size on Adsorption Behavior of Hydrogels for Dye*

Electrostatic attraction is the primary mechanism for dye adsorption on cellulose-based adsorbents (Guo et al., 2018; Qiao et al., 2021). Carboxylated CNF such as TCNF-based hydrogels adsorb cationic dyes such as methylene blue due to the strong electrostatic attraction between anionic carboxyl groups and cationic dyes (He et al., 2013; Wang et al., 2018; Yang et al., 2017). It is well established that pH plays a crucial role in influencing electrostatic attraction between dyes or metals and adsorbents (Chen et al., 2015) due to pH induced changes in the surface charge of TCNF. We investigated the effect of pH on the adsorption capability of these hydrogels and demonstrated that the highest adsorption occurred at pH 5.7, and when the PH is lower or higher than 5.7, the adsorption capability becomes less. as shown in Fig. 3. As reported previously, cellulose-based materials present the highest charge density at neutral pH, which also presented the highest adsorption capability for cationic methylene blue (Tan et al. 2016). When the pH is lower or higher than 7, the adsorption capability is reduced (Tan et al. 2016). However, other phenomena in the system are at play, such as entropic rearrangement of the adsorbed water and exchange with the dyes, hydrogen bonding development, among others, as demonstrated in this work. It was also found that the methylene blue dyes adsorption capability increased by 20.3% (from 64.5 to 77.6) mg/g at pH 5.7 when the average fibril length decreased from 508.7 nm to 369.4 nm or fibril diameter decreased from 56.8 to 45.3 after 12 h of hydrolysis. However, further hydrolysis to 24 h, did not have a significant

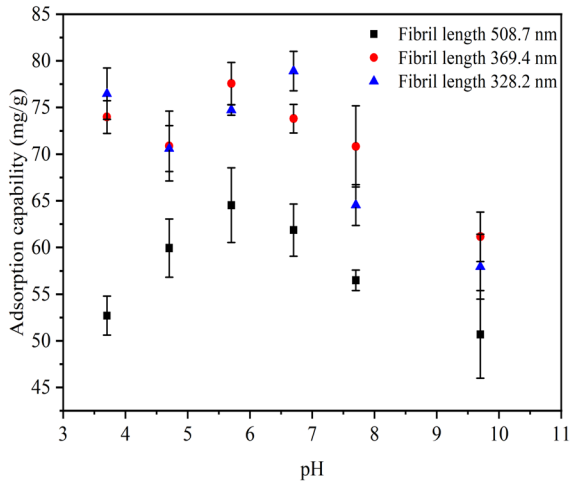

Fig. 3 The effect of fibril size on adsorption capability of TCNF hydrogels for methylene blue cationic dyes at different pH values. Each test was done by triplicates; averages and standard deviations were reported

effect on either adsorption capability or efficiency, perhaps due to smaller decreases in fibril length and diameter to 328.2 and 38.3, respectively. Additionally, pore saturation may also be a key influencing factor. Once the available pores within the hydrogel matrix become filled with adsorbates, further uptake is limited regardless of fibril size (Liu et al. 2021). Another important factor is surface charge redistribution during the adsorption process. As contaminants interact with hydrogel, especially charged species like cationic methylene dyes, the local electrostatic environment of the hydrogel surface may change. This can result in decreased electrostatic attraction over time, effectively passivating active sites and reducing further adsorption efficiency (Eckenrode et al. 2005). Both pore saturation and surface charge redistribution may occur in the case of hydrogels formed by TCNF after 12 h hydrolysis. Therefore, further hydrolysis to reduce the fibril size did not affect the adsorption efficiency and adsorption capability.

The adsorption kinetics was conducted using the data obtained at pH 5.7 with an initial methylene blue concentration of 200 mg/L (Fig. 4(A)). Data fitted to the pseudo-first-order and pseudo-second-order model as well as the intraparticle diffusion model (Fig. 4(B), (C), and (D)). The fitting parameters are listed in Table 2. The pseudo-second order model resulted in a similar R^2 value (0.9782, 0.9839,

0.9839) with in the case of the pseudo-first order model (0.9753, 0.9774, 0.9841) for hydrogels formed by TCNF of varying fibril size. The results indicate that electrostatic forces and hydrogen bonding might contribute to the adsorption. However, the contribution of each phenomenon is hard to estimate based only on R^2 values. The rate constant k2 followed the order k2 (12 h) ≈ k2 (24 h)> k2 (0 h), which suggests that TCNF hydrogel made of fibrils of length 369.4 nm and fibril diameter 45.3 nm achieved the greatest adsorption rate. Further decreasing fibril sizes (through endoglucanase treatment for 24 h) did not increase absorption rate.

The slopes of the three adsorption stages (as shown in Fig. 4(D)) were calculated from the intraparticle diffusion model and were summarized in Table 2. Interestingly, the hydrogels made of TCNF with smaller fibril sizes had a greater $K_{id,1}$, indicating that smaller particle size leads to an increase in adsorption rates through external surface adsorption. However, the adsorption capability and rates for hydrogels made of TCNFs treated with endoglucanase for 12 and 24 hours had no significant differences. Perhaps, the decreases in fibril length and diameter from 369.4 ± 12.1 nm to 328.2 ± 12.6 nm and from 45.3 ± 14.3 nm to 38.3 ± 13.1 nm, respectively, were not significant enough to enhance the adsorption ability.

The effect of the fibril size on the adsorption capability of TCNF hydrogels for anionic methyl blue

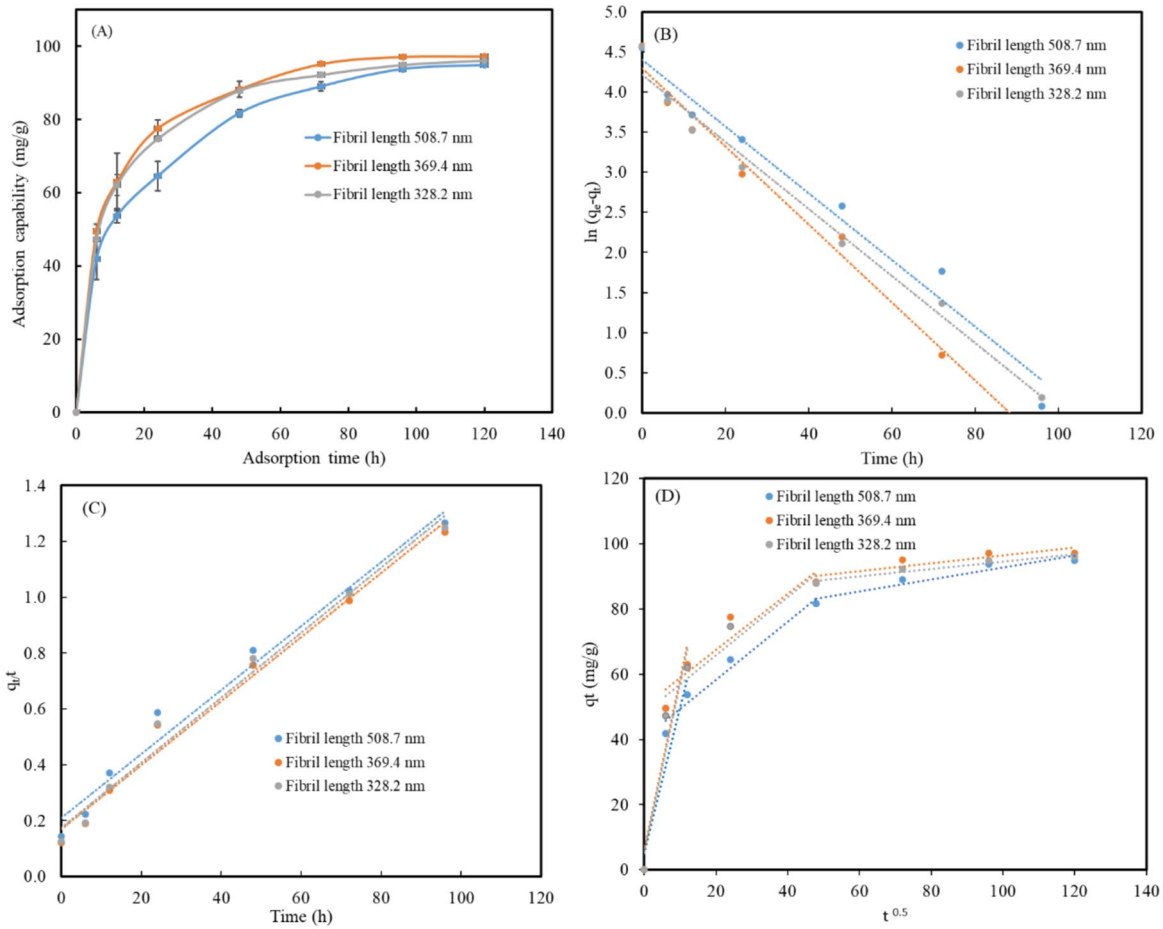

Fig. 4 **A** The adsorption kinetic of TCNF hydrogel for methylene blue (+) dyes at pH 5.7 with initial methylene blue concentration is 200 mg/L. **B** Data fitted to pseudo-first-order kinetics model, **C** pseudo-second-order kinetics model, and **D** intraparticle diffusion model. Each test was done by triplicates; averages and standard deviations were reported

Table 2 Parameters extracted from the pseudo-first-order, pseudo-second order, and Intra-particle diffusion models of TCNF hydrogel for methylene blue cationic dyes

Kinetic parameters	Enzyme hydrolysis 0 h	Enzyme hydrolysis 12 h	Enzyme hydrolysis 24 h
$q_{e,exp}$ (mg/g)	94.8	97.2	96.1
Pseudo-first-order			
q_e,cal (mg/g)	81.4916	94.9452	67.5657
K_1 (mg/(g*h))	0.0416	0.0635	0.0418
R^2	0.9753	0.9774	0.9841
Pseudo-second-order			
q_e,cal (mg/g)	87.7193	86.95652	86.2069
K_2 (mg/(g*h))	0.00062	0.00078	0.00077
R^2	0.9782	0.9839	0.9839
Intraparticle diffusion model			
$K_{id,1}$ (mg/(g*h))	4.47	5.24	5.18
c_1	5.03	6.00	5.39
R_1^2	0.9047	0.9016	0.9172
$K_{id,2}$ (mg/(g*h))	0.89	0.86	0.89
c_2	40.3.	50.24	47.95
R_2^2	0.9637	0.8883	0.9049
$K_{id,3}$ (mg/(g*h))	0.184	0.1202	0.1141
c_3	74.33	84.338	83.162
R_3^2	0.9092	0.7754	0.9408

dyes at different pH values was also investigated, as shown in Fig. 5(A). The adsorption capability was less than 10 mg/g (around 12.5 % of cationic methylene blue adsorption capability) and did not have significant difference in different pH values. In this case, TCNF hydrogel and anionic dyes all presented negative charges. Therefore, the total adsorption capability contributed from porous structural filling, hydrogen bonding, Van der Waals forces, hydrophobic-driven adsorption, π–π stacking, etc., which was less than 12.5% and independent on pH. This result further confirmed that the adsorption capability for the methylene cationic dyes mainly contributed from electrostatic attraction force (more than 87.5%), which depends on the pH. Additionally, the adsorption of TCNF hydrogels for the anionic methyl blue dyes was not affected by different fibril sizes (Fig. 5(B)).

To confirm the results above, the adsorption behavior of TCNF/PEI hydrogel formed from different fibril size TCNF for anionic methyl blue (Fig. S2, S3 and Table S1) and cationic methylene blue (Figure S4) were also tested. The results were similar with the TCNF hydrogel adsorption behavior for the cationic methylene blue and anionic methyl blue dues. Specifically, 1) the anionic methyl blue adsorption capability increased from 80.1 mg/g to 88.2 mg/g, increasing by 10.1% at pH 5.7 (Fig. S2(A)) when the fibril length decreased from 508.7 to 369.4 nm with fibril diameter decreased from 56.8 to 45.3 nm; 2) Adsorption rate of TCNF/PEI hydrogel for anionic methyl blue dyes were increased (hydrogel formed by suspensions with smaller fibril size resulted in higher Kid values, Fig. S2(D) and Table S1); 3) The adsorption capability of all those TCNF/PEI hydrogels for the cationic methylene blue dyes adsorption was less than 10 mg/g (take up 10.1 % of adsorption capability of TCNF/PEI hydrogel for anionic methyl blue) (Fig. S3). However, this adsorption performance didn't have significant change when the fibril length continued decreasing to 328.2 nm with fibril diameter decreased to 38.3 nm.

This work contributes evidence that the adsorption mechanism of cellulose-based adsorbents for cationic methylene dyes might be dominated by electrostatic attraction (up to 87.5%). Additional contributing mechanisms include porous structural filling, hydrogen bonding, Van der Waals forces, hydrophobic-driven adsorption, π–π stacking, etc. (Fig. 6).

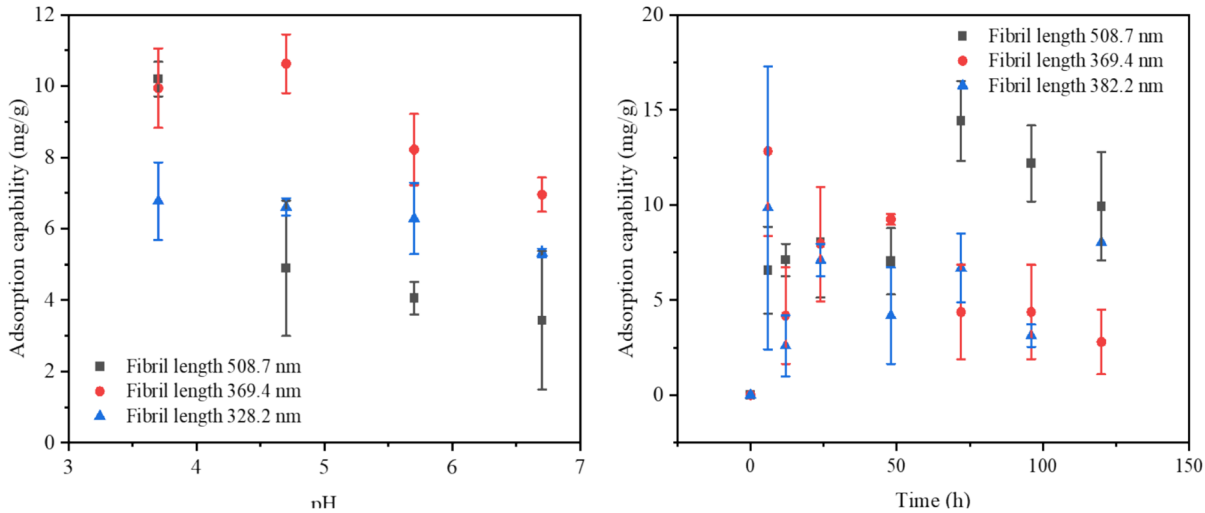

Fig. 5 The effect of different particle sizes on the adsorption capability of their TCNF hydrogel for anionic methyl blue dyes at different PH values (**A**) and with adsorption time change (**B**). Each test was done by triplicates to calculate standard deviation

4 Conclusions

This work demonstrated that CNF treatment using a commercial endoglucanase (FiberCare®) is a viable approach to change TCNF fibril size without affecting carboxyl groups content. Endoglucanase treatment increased TCNF zeta potential values and adsorption capability. Decreasing TCNF fibril size did not alter the adsorption mechanism of TCNF-PEI hydrogels but increased the overall adsorption rates based on the adsorption kinetic model and intra-particle diffusion model. The study reveals that decreasing TCNF fibril size enhances both adsorption capability and overall adsorption rate. However, further fibrillation is not necessary as the adsorption capability and rate no longer significantly increase after 12 h hydrolysis. Additionally, adsorption capability for the dyes mainly contributed from electrostatic attraction force (more than 87.5%), which depends on the pH. While the

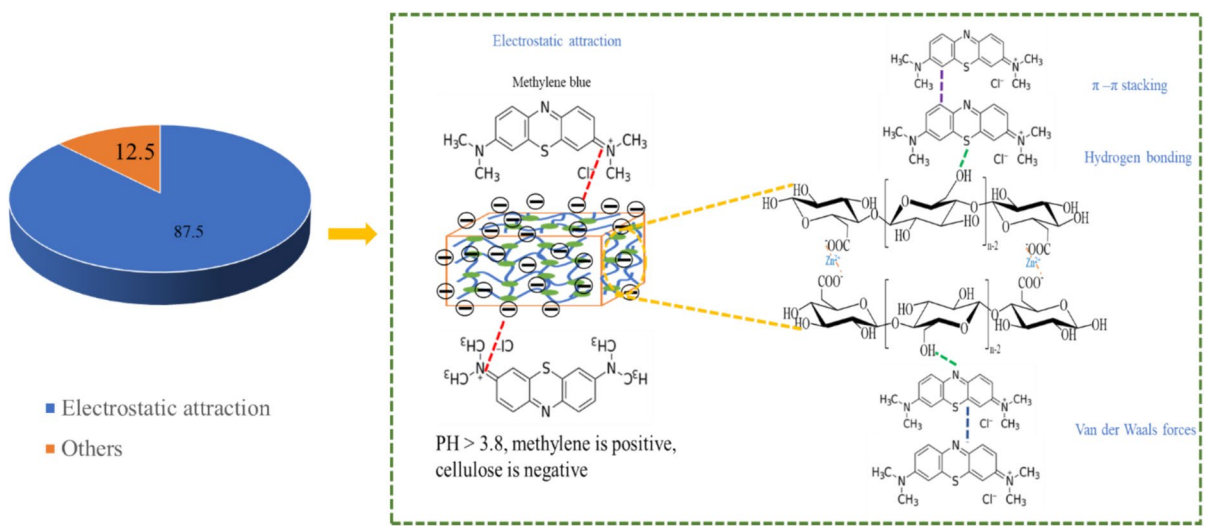

Fig. 6 The adsorption mechanism of TCNF hydrogel for cationic methylene blue dyes

total adsorption capability contributed from porous structural filling, hydrogen bonding, Van der Waals forces, hydrophobic-driven adsorption, π–π stacking, etc. was less than 12.5%, which independent on pH. This study provides a green method to reduce nanocellulose fibril size for optimized adsorption performance. The use of a commercially available enzyme (FiberCare®) offers a cost-effective and environmentally friendly method for turning CNF properties, which is favorable for industrial adoption.

Acknowledgements Not applicable

CRediT Authorship Contribution Statement Yufei Nan: Conceptualization, Methodology, Investigation, Formal Analysis, Visualization, Writing – original draft; Diego Gomez-Maldonado: Conceptualization, Methodology, Formal Analysis, Visualization, Writing – review & editing; Fatimatu Bello: Formal analysis, Visualization, Writing – review & editing; Junyong Zhu: Methodology, Writing – review & editing; Maria S. Peresin: Conceptualization, Methodology, Visualization, Supervision, Funding acquisition, Writing – review and editing.

Declaration of Generative AI in Scientific Writing During the preparation of this work the author(s) used ChatGPT to correct grammatical errors and improve readability. After using this tool/service, the author(s) reviewed and edited the content as needed and take(s) full responsibility for the content of the published article.

Funding This work was supported by the National Science Foundation CAREER award (2119809) through the BMAT program in the Division of Materials Research and the EPSCoR program. Likewise, the USDA National Institute of Food and Agriculture, Hatch program (ALA013-17003), and McIntire-Stennis program (1022526) are acknowledged for the support of this work. The authors also want to acknowledge the support from Chinese Scholarship Council (201906300036).

Data Availability Data is available upon reasonable request to authors.

Declarations

Ethics Approval and Consent to Participate Not applicable

Consent for Publication Not applicable.

Competing Interest The authors declare that the research was conducted in the absence of any commercial or financial relationships that could be construed as a potential conflict of interest.

References

Bello, F., & Peresin, M. S. (2024). Multifunctional pectin and lignin-containing cellulose nanofiber films with improved UV resistance and mechanical properties. *Food Hydrocolloids, 157*, 110378. https://doi.org/10.1016/j.foodhyd.2024.110378

Bradford, M. M. (1976). A rapid and sensitive method for the quantitation of microgram quantities of protein utilizing the principle of protein-dye binding. *Analytical Biochemistry, 72*, 248–254. https://doi.org/10.1016/0003-2697(76)90527-3

Chen, T., Zhou, Z., Han, R., Meng, R., Wang, H., & Lu, W. (2015). Adsorption of cadmium by biochar derived from municipal sewage sludge: Impact factors and adsorption mechanism. *Chemosphere, 134*, 286–293. https://doi.org/10.1016/j.chemosphere.2015.04.052

Eckenrode, H. M., Jen, S. H., Han, J., Yeh, A. G., & Dai, H. L. (2005). Adsorption of a cationic dye molecule on polystyrene microspheres in colloids: Effect of surface charge and composition probed by second harmonic generation. *The Journal of Physical Chemistry B, 109*(10), 4646–4653. https://doi.org/10.1021/jp045610q

Esmaeili, Z., Izadyar, S., Hamzeh, Y., & Abdulkhani, A. (2021). Preparation and characterization of highly porous cellulose nanofibrils/chitosan aerogel for acid blue 93 adsorption: Kinetics, isotherms, and thermodynamics analysis. *Journal of Chemical & Engineering Data, 66*(2), 1068–1080. https://doi.org/10.1021/acs.jced.0c00872

Gu, J., Zhao, Y., Guan, Y., & Zhang, Y. (2015). Effect of particle size in a colloidal hydrogel scaffold for 3D cell culture. *Colloids and Surfaces B: Biointerfaces, 136*, 1139–1147. https://doi.org/10.1016/j.colsurfb.2015.11.021

Guo, D.-M., An, Q.-D., Li, R., Xiao, Z.-Y., & Zhai, S.-R. (2018). Ultrahigh selective and efficient removal of anionic dyes by recyclable polyethylenimine-modified cellulose aerogels in batch and fixed-bed systems. *Colloids and Surfaces A: Physicochemical and Engineering Aspects, 555*, 150–160. https://doi.org/10.1016/j.colsurfa.2018.06.081

Habibi, Y., Lucia, L. A., & Rojas, O. J. (2010). Cellulose nanocrystals: Chemistry, self-assembly, and applications.

Chemical Reviews, 110, 3479–3500. https://doi.org/10.1021/cr900339w

Han, J., Zhou, C., Wu, Y., Liu, F., & Wu, Q. (2013). Self-assembling behavior of cellulose nanoparticles during freeze-drying: Effect of suspension concentration, particle size, crystal structure, and surface charge. *Biomacromolecules, 14*, 1529–1540. https://doi.org/10.1021/bm4001734

He, X., Male, K. B., Nesterenko, P. N., Brabazon, D., Paull, B., & Luong, J. H. (2013). Adsorption and desorption of methylene blue on porous carbon monoliths and nanocrystalline cellulose. *ACS Applied Materials & Interfaces, 5*, 8796–8804. https://doi.org/10.1021/am403222u

Hoeger, I. C., Nair, S. S., Ragauskas, A. J., Deng, Y., Rojas, O. J., & Zhu, J. (2013). Mechanical deconstruction of lignocellulose cell walls and their enzymatic saccharification. *Cellulose, 20*, 807–818. https://doi.org/10.1007/s10570-013-9867-9

Hubbe, M. A., & Grigsby, W. (2020). From nanocellulose to wood particles: A review of particle size vs. the properties of plastic composites reinforced with cellulose-based entities. *Bioresources, 15*, 2030–2081. https://doi.org/10.15376/BIORES.15.1.2030-2081

Hubbe, M. A., Rojas, O. J., Lucia, L. A., & Sain, M. (2008). Cellulosic nanocomposites: a review. *Bioresources, 3*, 929–980.

Isogai, A. (2021). Emerging nanocellulose technologies: Recent developments. *Advanced Materials, 33*, 2000630. https://doi.org/10.1002/adma.202000630

Kapoor, M., Semwal, S., Satlewal, A., Christopher, J., Gupta, R. P., Kumar, R., Puri, S. K., & Ramakumar, S. (2019). The impact of particle size of cellulosic residue and solid loadings on enzymatic hydrolysis with a mass balance. *Fuel, 245*, 514–520. https://doi.org/10.1016/j.fuel.2019.02.094

Kaur, P., Sharma, N., Munagala, M., Rajkhowa, R., Aallardyce, B., Shastri, Y., & Agrawal, R. (2021). Nanocellulose: Resources, physio-chemical properties, current uses and future applications. *Frontiers in Nanotechnology, 3*, 747329. https://doi.org/10.3389/fnano.2021.747329

Khalid, M. Y., Al Rashid, A., Arif, Z. U., Ahmed, W., & Arshad, H. (2021). Recent advances in nanocellulose-based different biomaterials: Types, properties, and emerging applications. *Journal of Materials Research and Technology, 14*, 2601–2623. https://doi.org/10.1016/j.jmrt.2021.07.128

Liu, W., Zhang, Y., Wang, S., Bai, L., Deng, Y., & Tao, J. (2021). Effect of pore size distribution and amination on adsorption capacities of polymeric adsorbents. *Molecules, 26*(17), 5267. https://doi.org/10.3390/molecules26175267

Lou, H., Zhu, J. Y., Lan, T. Q., Lai, H., & Qiu, X. (2013). pH-Induced lignin surface modification to reduce nonspecific cellulase binding and enhance enzymatic saccharification of lignocelluloses. *ChemSusChem, 6*(5), 919–927. https://doi.org/10.1002/cssc.201200859

Mishra, R. K., Sabu, A., & Tiwari, S. K. (2018). Materials chemistry and the futurist eco-friendly applications of nanocellulose: Status and prospect. *Journal of Saudi Chemical Society, 22*, 949–978. https://doi.org/10.1016/j.jscs.2018.02.005

Nair, S. S., Zhu, J., Deng, Y., & Ragauskas, A. J. (2014). High performance green barriers based on nanocellulose. *Sustainable Chemical Processes, 2*, 1–7. https://doi.org/10.1186/s40508-014-0023-0

Nan, Y., Gomez-Maldonado, D., Iglesias, M. C., Whitehead, D. C., & Peresin, M. S. (2023a). Valorized soybean hulls as TEMPO-oxidized cellulose nanofibril and polyethylenimine composite hydrogels and their potential removal of water pollutants. *Cellulose, 30*, 3639–3651. https://doi.org/10.1007/s10570-023-05086-y

Nan, Y., Gomez-Maldonado, D., Whitehead, D. C., Yang, M., & Peresin, M. S. (2023b). Comparison between nanocellulose-polyethylenimine composites synthesis methods towards multiple water pollutants removal: A review. *International Journal of Biological Macromolecules, 232*, 123342. https://doi.org/10.1016/j.ijbiomac.2023.123342

Nan, Y., Gomez-Maldonado, D., Zhang, K., Du, H., Whitehead, D. C., Li, M., Zhang, X., & Peresin, M. S. (2024). Polyethylenimine functionalized graphene oxide and cellulose nanofibril composite hydrogels: Synthesis, characterization and water pollutants adsorption. *Carbohydrate Polymer Technologies and Applications, 8*, 100585. https://doi.org/10.1016/j.carpta.2024.100585

Nogi, M., Iwamoto, S., Nakagaito, A. N., & Yano, H. (2009). Optically transparent nanofiber paper. *Advanced Materials, 21*, 1595–1598. https://doi.org/10.1002/adma.200803174

Qiao, A., Cui, M., Huang, R., Ding, G., Qi, W., He, Z., Klemeš, J. J., & Su, R. (2021). Advances in nanocellulose-based materials as adsorbents of heavy metals and dyes. *Carbohydrate Polymers, 272*, 118471. https://doi.org/10.1016/j.carbpol.2021.118471

Saito, T., & Isogai, A. (2004). TEMPO-mediated oxidation of native cellulose. The effect of oxidation conditions on chemical and crystal structures of the water-insoluble fractions. *Biomacromolecules, 5*, 1983–1989. https://doi.org/10.1021/bm0497769

Saito, T., Hirota, M., Tamura, N., Kimura, S., Fukuzumi, H., Heux, L., & Isogai, A. (2009). Individualization of nanosized plant cellulose fibrils by direct surface carboxylation using TEMPO catalyst under neutral conditions. *Biomacromolecules, 10*, 1992–1996. https://doi.org/10.1021/bm900414t

Sehaqui, H., Berglund, L. A., & Zhou, Q. (2013). BIOREFINERY: Nanofibrillated cellulose for enhancement of strength in high-density paper structures. *Nordic Pulp & Paper Research Journal, 28*, 182–189. https://doi.org/10.3183/npprj-2013-28-02-p182-189

Tan, K. B., Abdullah, A. Z., Horri, B. A., & Salamatinia, B. (2016). Adsorption Mechanism of Microcrystalline Cellulose as Green Adsorbent for the Removal of Cationic Methylene Blue Dye. *Journal of the Chemical Society of Pakistan, 38*(4).

Wang, D., Yu, H., Fan, X., Gu, J., Ye, S., Yao, J., & Ni, Q. (2018). High aspect ratio carboxylated cellulose nanofibers cross-linked to robust aerogels for superabsorption–flocculants: Paving way from nanoscale to macroscale. *ACS Applied Materials & Interfaces, 10*, 20755–20766. https://doi.org/10.1021/acsami.8b04211

Wang, H., Zhu, J. J., Ma, Q., Agarwal, U. P., Gleisner, R., Reiner, R., Baez, C., & Zhu, J. (2020). Pilot-scale

production of cellulosic nanowhiskers with similar morphology to cellulose nanocrystals. *Frontiers in Bioengineering and Biotechnology, 8*, 565084. https://doi.org/10.3389/fbioe.2020.565084

Yang, W., Zheng, F., Xue, X., & Lu, Y. (2011). Investigation into adsorption mechanisms of sulfonamides onto porous adsorbents. *Journal of Colloid and Interface Science, 362*, 503–509. https://doi.org/10.3389/fbioe.2020.565084

Yang, X., Liu, H., Han, F., Jiang, S., Liu, L., & Xia, Z. (2017). Fabrication of cellulose nanocrystal from Carex meyeriana Kunth and its application in the adsorption of methylene blue. *Carbohydrate Polymers, 175*, 464–472. https://doi.org/10.1016/j.carbpol.2017.08.007

Yu, Z., Hu, C., Dichiara, A. B., Jiang, W., & Gu, J. (2020). Cellulose nanofibril/carbon nanomaterial hybrid aerogels for adsorption removal of cationic and anionic organic dyes. *Nanomaterials, 10*(1), 169. https://doi.org/10.3390/nano10010169

Zhang, K.-Y., Li, D., Wang, Y., & Wang, L.-J. (2023). Carboxymethyl chitosan/polyvinyl alcohol double network hydrogels prepared by freeze-thawing and calcium chloride cross-linking for efficient dye adsorption. *International Journal of Biological Macromolecules, 253*, 126897. https://doi.org/10.1016/j.ijbiomac.2023.126897

Zhang, Z., Wang, F., Yang, W., Yang, Z., & Li, A. (2016). A comparative study on the adsorption of 8-amino-1-naphthol-3, 6-disulfonic acid by a macroporous amination resin. *Chemical Engineering Journal, 283*, 1522–1533. https://doi.org/10.1016/j.cej.2015.08.010

Zhu, H., Luo, W., Ciesielski, P. N., Fang, Z., Zhu, J., Henriksson, G., Himmel, M. E., & Hu, L. (2016). Wood-derived materials for green electronics, biological devices, and energy applications. *Chemical Reviews, 116*, 9305–9374. https://doi.org/10.1016/j.chemosphere.2015.04.052

Zhu, J., & Agarwal, U. P. (2022). *Nanocellulose: Native state, production, and characterization, Emerging nanotechnologies in nanocellulose* (pp. 1–39). Springer. https://doi.org/10.1007/978-3-031-14043-3_1